J|A|C|S
ARTICLES
Published on Web 12/06/2006

On the Mechanism of an Asymmetric α,β-Unsaturated Carboxylic Acid Hydrogenation: Application to the Synthesis of a PGD_2 Receptor Antagonist

David M. Tellers,* J. Christopher McWilliams, Guy Humphrey, Michel Journet, Lisa DiMichele, Joseph Hinksmon, Arlene E. McKeown, Thorsten Rosner, Yongkui Sun, and Richard D. Tillyer

Contribution from the Department of Process Research, Merck and Co., Inc., P.O. Box 2000, Rahway, New Jersey 07065-0900

Received April 18, 2006; E-mail: david_tellers@merck.com

Abstract: Ruthenium complexes employing axially chiral ligands were found to be effective asymmetric hydrogenation catalysts for the reduction of α,β-unsaturated ene acid **1-E** to give **2**, a prostaglandin D_2 (PGD_2) receptor antagonist. With $[(S\text{-BINAP})Ru(p\text{-cymene})Cl_2]_2$ (**3**, *S*-BINAP = (*S*)-(+)-2,2′-bis(diphenylphospino)-1,1′-binapthyl), it was discovered that low hydrogen pressures (<30 psi) were essential to achieve high enantioselectivities (92% ee). A detailed mechanistic study was undertaken to elucidate this pressure dependence. It was determined that compound **1-E** is in a ruthenium-catalyzed equilibrium with endocylic isomer **1-Endo** and in photochemical equilibrium with *Z* isomer **1-Z**. Each isomer could be hydrogenated to give **2**, albeit with different rates and enantioselectivities. Hydrogenation of **1-Endo** with **3** was found to give **2** in high enantiomeric excess, regardless of pressure and at a rate substantially faster than that of hydrogenation of **1-E** and **1-Z**. In contrast, isomers **1-E** and **1-Z** exhibited pressure-dependent enantioselectivities, with higher enantiomeric excesses obtained at lower pressures. A rationale for this pressure dependence is described. Deuterium labeling studies with **1-Endo** and tiglic acid were used to elucidate the mechanism of hydride insertion and product release from ruthenium. Under neutral conditions, protonolysis was the major pathway for metal−carbon cleavage, while under basic conditions, hydrogenolysis of the metal−carbon bond was predominant.

Introduction

Asymmetric hydrogenation of unsaturated substrates is arguably the most useful synthetic method for introducing chirality into a molecule.[1,2] In recent years, the number of applications, chiral ligands, and commercial suppliers in this field has grown dramatically.[3] Despite this, the application of asymmetric hydrogenation to pharmaceutically relevant molecules has been somewhat limited.[3−6] Reasons for this include the cost of the catalytic route vs the racemic route, the availability of the ligand on a large scale, and the difficulty associated with handling air-sensitive catalysts in conjunction with hydrogen gas. Nonetheless, our laboratories have recently focused our efforts on implementing catalytic asymmetric hydrogenation into synthetic processes.[7−12] In addition to the environmental benefits obtained from using this atom-efficient chemistry, we believe that incorporation of asymmetric hydrogenation will, in many cases, allow for the development of more efficient, economic, and elegant syntheses.

Indole **2** has been identified as a prostaglandin D_2 (PGD_2) receptor antagonist (Figure 1).[13,14] It is thought that excess production of PGD_2 causes the inflammation observed in allergic diseases. In order to fully investigate this effect, we required a practical and efficient synthesis of **2.** Toward that end, we postulated that asymmetric hydrogenation could serve as a useful method for introducing chirality into indole **2**.[15−18]

(1) Tang, W.; Zhang, X. *Chem. Rev.* **2003**, *103*, 3029−3069.
(2) Noyori, R.; Ohkuma, T. *Angew. Chem., Int. Ed.* **2001**, *40*, 40−73.
(3) Blaser, H.-U.; Spindler, F.; Thommen, M.; Blaser, H. U.; F. S., Thommen, M. Industrial Applications. In *Handbook of Homogeneous Hydrogenation*; de Vries, J.G., Elsevier, C. J., Eds.; Wiley-VCH: Weinheim, Germany, 2006.
(4) Blaser, H.-U.; Malan, C.; Pugin, B.; Spindler, F.; Steiner, H.; Studer, M. *Adv. Synth. Catal.* **2003**, *345*, 103−151.
(5) Thayer, A. *Chem. Eng. News.* **2005**, *36*, 40−48.
(6) Hawkins, J. M.; Watson, T. J. N. *Angew. Chem., Int. Ed.* **2004**, *43*, 3224−3228.
(7) Hsiao, Y.; Rivera, N.; Rosner, T.; Krska, S. W.; Njolita, E.; Wang, F.; Sun, Y.; Armstrong, I., J. D.; Grabowski, E. J. J.; Tillyer, R. D.; Spindler, F.; Malan, C. *J. Am. Chem. Soc.* **2004**, *126*, 9918−9919.
(8) Ikemoto, N.; Tellers, D. M.; Dreher, S. D.; Liu, J.; Huang, A.; Rivera, N.; Njolita, E.; Hsiao, Y.; McWilliams, J. C.; Williams, J. M.; Armstrong, J. D., III; Sun, Y.; Mathre, D.; Grabowski, E. J. J.; Tillyer, R. D. *J. Am. Chem. Soc.* **2004**, *126*, 3048−3049.
(9) Maligres, P. E.; Krska, S. W.; Humphrey, G. R. *Org. Lett.* **2004**, *6*, 3147−3150.
(10) Shultz, C. S.; Dreher, S. D.; Ikemoto, N.; Williams, J. M.; Grabowski, E. J. J.; Krska, S. W.; Sun, Y.; Dormer, P. G.; DiMichele, L. *Org. Lett.* **2005**, *7*, 3405−3408.
(11) Tellers, D. M.; Bio, M.; Song, Z. J.; McWilliams, J. C.; Sun, Y. *Tetrahedron: Asymmetry* **2006**, *17*, 550−553.
(12) Hansen, K. B.; Rosner, T.; Kubryk, M.; Dormer, P. G.; Armstrong, J. D., III. *Org. Lett.* **2005**, *7*, 4935−4938.
(13) Sturino, C. F.; Lachance, N.; Berthelette, C.; Li, L.; Wang, Z. U.S. Patent 0124680, 2005.
(14) Sturino, C. F.; et al. *J. Med. Chem.* **2006**, in press.

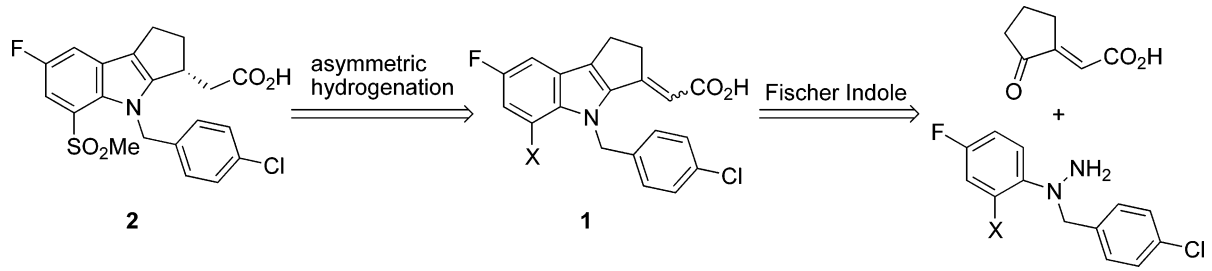

Figure 1. Retrosynthetic analysis of **2**.

The retrosynthetic analysis of **2**, presented in Figure 1, relies upon construction of the prochiral indole α,β-unsaturated acid **1** via a Fischer indole reaction. Subsequent asymmetric hydrogenation of intermediate **1** would yield chiral acid **2**. Key to the successful implementation of this process was the identification of a catalyst which was readily accessible and could be employed at relatively low loading. In addition to these practical constraints, to the best of our knowledge, asymmetric hydrogenation of α,β-unsaturated acids similar to **1** has not been reported.[19−25] In particular, the exocyclic ene acid functionality coupled with the indole framework makes **1** a unique asymmetric hydrogenation target. Surprisingly, a broader examination of the literature revealed that there were no examples of asymmetric hydrogenation of exocyclic α,β-unsaturated acids. Herein we describe the enantioselective hydrogenation of trisubstituted olefin **1**. Details of the synthesis of **2** will be reported elsewhere.[26]

Results and Discussion

1. Reaction Discovery, Optimization, and Implementation. A. Substrate and Catalyst Identification. Efforts to identify a suitable hydrogenation catalyst were performed in parallel with the development of the synthesis of chiral acid **2**. Consequently, our initial screening efforts focused on discovering a hydrogenation catalyst for **1-Br-E** (eq 1), a readily available intermediate at the time.[27]

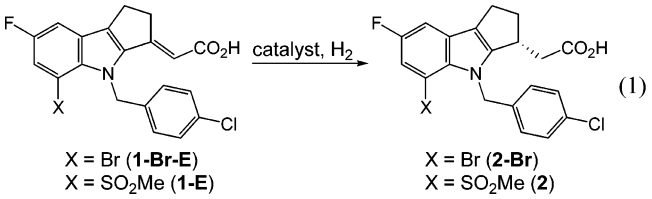

Based upon literature precedence, α,β-unsaturated carboxylic acids can be hydrogenated in alcoholic solvents with both ruthenium and rhodium catalysts to produce the corresponding chiral acid with good enantioselectivity.[1,28,29] As such, ene acid **1-Br-E** was screened against rhodium and ruthenium catalysts prepared from our chiral ligand library at the practical hydrogen pressure of 105 psi. Preliminary screening reactions in methanol with the free acid showed little reactivity. This was likely a result of the poor solubility of **1-Br-E** in MeOH (1.7×10^{-4} M at 22 °C).[30] In order to improve the solubility, subsequent hydrogenations were performed with the more soluble triethylamine salt of **1-Br-E** (1.8×10^{-2} M at 22 °C). Under these conditions, we were pleased to find that both rhodium and ruthenium catalysts provided **2-Br** with good enantioselectivity. Selected data from this screen are presented in Table 1. Ruthenium catalysts employing axial chiral ligands, like BINAP, gave the best reactivity and enantioselectivity. In general, catalysts derived from rhodium were substantially less reactive and enantioselective than ruthenium catalysts under the conditions examined.[1] We were encouraged by the results from this initial screen, as it demonstrated that asymmetric hydrogenation could serve as a useful means for preparing **2**, as envisioned in Figure 1.

Table 1. Selected Hydrogenation Results with **1-Br-E** and **1-E**[a]

entry	substrate	ligand[b]	metal precursor	%ee
1	**1-Br-E**	*R*-BINAP	$[Ru(p\text{-cymene})Cl_2]_2$	−85
2	**1-E**	*R*-BINAP	$[Ru(p\text{-cymene})Cl_2]_2$	−84
3	**1-Br-E**	*R*-xylBINAP	$[Ru(p\text{-cymene})Cl_2]_2$	−87
4	**1-E**	*R*-xylBINAP	$[Ru(p\text{-cymene})Cl_2]_2$	−87
5	**1-E**	*R*-Cl-MeO-BIPHEP	$[Ru(p\text{-cymene})Cl_2]_2$	−81
6	**1-E**	*R*-*N*-MeSolphos	$[Ru(p\text{-cymene})Cl_2]_2$	−83
7	**1-Br-E**	(+)-TMBTP	$Rh(COD)_2BF_4$	−87
8	**1-Br-E**	(*S*,*S*)-f-BINAPHANE	$Rh(COD)_2BF_4$	85

[a] Conditions: 105 psi H_2, 50 °C, MeOH, triethylamine (100 mol %), catalyst (10 mol %), [substrate] = 2.3×10^{-2} M. All reactions gave >99 area % conversion (HPLC 215 nm) except for entry 8 (88 HPLC area % conversion at 215 nm). [b] See Supporting Information for structures of ligands.

During hydrogenation screening of **1-Br-E**, an efficient, high-yielding synthesis of sulfone ene acid **1-E** was developed.[26] Hydrogenation of **1-E** serves to set the stereocenter as the last step in the chemical synthesis, thereby avoiding the loss of

(15) Methods have been reported for setting the chiral center in **2**. See refs 16−18.
(16) Campos, K. R.; Journet, M.; Lee, S.; Grabowski, E. J. J.; Tillyer, R. D. *J. Org. Chem.* **2005**, *70*, 268−274.
(17) Shafiee, A.; Upadhyay, V.; Corley, E. G.; Biba, M.; Zhao, D.; Marcoux, J.-F.; Campos, K. R.; Journet, M.; King, A. O.; Larsen, R. D.; Grabowski, E. J. J.; Volante, R. P.; Tillyer, R. D. *Tetrahedron: Asymmetry* **2005**, *16*, 3094−3098.
(18) Hillier, M. C.; Marcoux, J.-F.; Zhao, D.; Grabowski, E. J. J.; McKeown, A. E.; Tillyer, R. D. *J. Org. Chem.* **2005**, *70*, 8385−8394.
(19) For a diastereoselective heterogeneous hydrogenation of an indole α,β-unsaturated ester, see: Beard, R. L.; Meyers, A. I. *J. Org. Chem.* **1991**, *56*, 2091−2096.
(20) For a diastereoselective homogeneous exocyclic α,β-unsaturated ester, see: Ohba, M.; Haneishi, T.; Fujii, T. *Heterocycles* **1994**, *38*, 2253−2265.
(21) For examples of asymmetric exocyclic dehydroamino acid hydrogenations, see refs 22−25.
(22) Jiang, X.; van den Berg, M.; Minnaard, A. J.; Feringa, B. L.; de Vries, J. G. *Tetrahedron: Asymmetry* **2004**, *15*, 2223−2229.
(23) Imamoto, T.; Oohara, N.; Takahashi, H. *Synthesis* **2004**, *9*, 1353−1358.
(24) Oohara, N.; Katagiri, K.; Imamoto, T. *Tetrahedron: Asymmetry* **2003**, *14*, 2171−2175.
(25) Ohashi, A.; Kikuchi, S.; Yasutake, M.; Imamoto, T. *J. Org. Chem.* **2002**, *15*, 2535−2546.
(26) Humphrey, G. R.; et al. Manuscript in preparation.
(27) Preliminary screening was also performed with the methyl ester of **1-Br**. In dichlorobenzene, this compound could be hydrogenated with (*R*)-(*S*)-Ph_2P-F-C-P(tBu)$_2$Rh(COD)BF_4 to give the corresponding chiral ester in 88% ee.
(28) Ratovelomanana-Vidal, V.; Genêt, J.-P. *J. Org. Chem.* **1998**, *59*, 163−171.
(29) Ohta, T.; Takaya, H.; Kitamura, M.; Nagai, K.; Noyori, R. *J. Org. Chem.* **1987**, *52*, 3176−3178.
(30) Compound **1** exhibited poor solubility in most solvents at room temperature. A detailed list of solubilities can be found in the Supporting Information.

valuable chiral intermediates. In addition, asymmetric reduction of **1-E**, as opposed to **1-Br-E**, supported the overall convergent synthetic pathway defined by our project team.[26,31] Consequently, emphasis was shifted toward identifying a catalyst suitable for hydrogenation of **1-E** (eq 1, X = SO_2Me).

A screening protocol identical to that employed for **1-Br-E** was performed with **1-E** using only catalysts derived from ruthenium. Selected results from this screen are presented in Table 1. In general, the replacement of the bromide for the sulfone had little impact on enantioselectivity. Again, axially chiral ligands gave **2** with the highest enantiomeric excess. In particular, (*R*-BINAP)(*p*-cymene)$RuCl_2$ and (*R*-xylBINAP)(p-cymene)$RuCl_2$ produced **2** in −84% and −87% ee, respectively. Given the project development timeline, we initially focused on optimizing the hydrogenation with (*S*-BINAP)(*p*-cymene)-$RuCl_2$ (**3**),[32] which was prepared in situ from [Ru(*p*-cymene)-Cl_2]$_2$ and *S*-BINAP, a readily available ligand.[33−36] It is presumed that **3** liberates *p*-cymene during the hydrogenation reaction to generate an active catalyst similar to (*S*-BINAP)-RuX_2 (X = Cl, OAc).[37] This is supported by the fact that hydrogenations performed with either **3** or (*S*-BINAP)RuX_2 (X = Cl, OAc) produce **2** with the same enantiomeric excess.

B. Hydrogenation Optimization. With a suitable catalyst in hand, development efforts focused on optimizing the hydrogenation such that it could be reproducibly performed on a multiple kilogram scale in a cost-effective manner. Our first attempt at addressing this goal focused on improving the solubility of ene acid **1-E**. At useful substrate concentrations (>0.20 M), hydrogenation mixtures were thick slurries, even in the presence of stoichiometric amounts of triethylamine. Preliminary reactions performed under these conditions were sluggish and irreproducible. In addition to the practical issues associated with handling thick slurries, we postulated that this limited solubility would likely attenuate reactivity; i.e., the reaction rate would be limited by substrate solubility, not by the inherent reactivity of the substrate. In order to increase the solubility of **1-E**, salts derived from **1-E** and 28 different bases were prepared and their solubilities measured. In general, salts prepared from strong organic bases (collidine, TMG) and inorganic bases containing large cations (KO^{t}Bu, Cs_2CO_3) exhibited the best solubilities. We decided to focus on the use of tetramethylguanidine (TMG) since it had been independently demonstrated that, under appropriate conditions, solutions of **2·TMG** could be crystallized in high optical purity. For example, **2·TMG** with an enantiomeric excess of 80% could be crystallized once to provide **2·TMG** in 99% ee. This crystallization allowed us to meet the strict optical purity requirements necessary for this compound, even if the asymmetric hydrogenation proceeded in less than 99% ee. All subsequent hydrogenations were therefore performed with **1-E·TMG** prepared either by in situ addition of stoichiometric TMG to the hydrogenation mixture or by crystallization and isolation prior to hydrogenation. Under these conditions, hydrogenation of **1-E·TMG** with (*S*-BINAP)Ru(*p*-cymene)Cl_2 (**3**) produced **2·TMG** in 84% ee and 97% assay yield (eq 2).[38] With **1-E·TMG** prepared in situ, catalyst loadings >0.8 mol % were required to obtain >95% conversion,[39] whereas with crystallized **1-E·TMG**, loadings as low as 0.3 mol % gave complete conversion. It is likely that crystallization serves to remove catalyst poisons produced during the synthesis of **1-E**. With the appropriate base in hand, we began to optimize additional reaction variables.

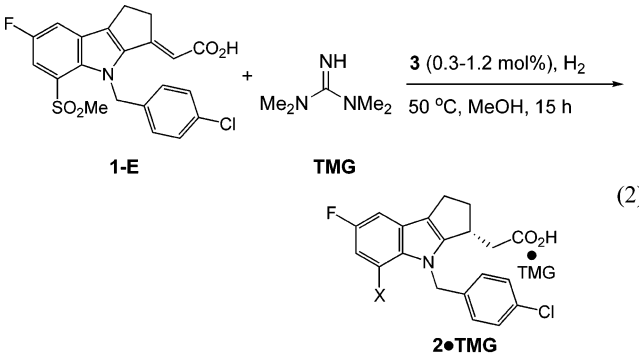

(2)

A key discovery was made when the effects of pressure and temperature were examined (Figure 2). We were surprised to find that the reaction enantioselectivity improved with *decreasing* hydrogen pressure. At 25 psi H_2, saturated acid **2** was obtained in 92% ee, while at 515 psi H_2, saturated acid **2** was obtained in 47% ee (Figure 2a). The inverse correlation between ee and pressure was also observed at different temperatures, with lower pressures giving higher enantioselectivites (Figure 2b). Interestingly, at 65 and 105 psi, 40 °C appeared to give the optimum enantioselectivity, whereas at 25 psi, temperature had a less pronounced effect on enantioselectivity. Most importantly, an increase of nearly 10% enantiomeric excess was achieved by simply lowering the hydrogen pressure from 105 to 35 psi (Table 2). On the basis of these data, 25−35 psi H_2 pressure and a reaction temperature of 50 °C were selected, as they offered the best compromise between rate and enantioselectivity (eq 2, 35 psi H_2). Importantly, at this lower pressure, little impact on rate was observed, with >99.9 area % conversion[39] obtained in <15 h. These conditions were successfully employed on a 1.2 kg scale in our hydrogenation facility. Details can be found in the Experimental Section.

It is important to note that hydrogenation of **1-E** represents one of a handful of homogeneous asymmetric α,β-unsaturated ene acid hydrogenations used to prepare pharmaceutical intermediates.[3,5] Mechanistic work on these hydrogenations has not been reported. Furthermore, the majority of literature examples of asymmetric ene acid hydrogenations describing either ligand

(31) Synthesis of **1-Br-E** employing the chemistry used to prepare **1-E** results in 10−30% debromination.
(32) Mashima, K.; Kusano, K.; Sato, N.; Matsumura, Y.; Nozaki, K.; Kumobayashi, H.; Sayo, N.; Hori, Y.; Ishizaki, T.; Akutagawa, S.; Takaya, H. *J. Org. Chem.* **1994**, *59*, 3064−3076.
(33) For reviews on the application of BINAP and its derivatives to asymmetric catalysis, see refs 34−36.
(34) Noyori, R.; Takaya, H. *Acc. Chem. Res.* **1990**, *23*, 345−350.
(35) Kumobayashi, H.; Miura, T.; Sayo, N.; Saito, T.; Zhang, X. *Synlett* **2001**, 1055.
(36) Akutagawa, S. *Appl. Catal. A* **1995**, *128*, 171−207.
(37) This is supported by the NMR spectroscopic observation that thermolysis of **3** in the presence of stoichiometric **1-E** liberates *p*-cymene over ca. 6 min.
(38) Assay yields were determined by preparing a known concentration of analytically pure **2** and comparing the UV response (HPLC) of this solution against that of a hydrogenation reaction solution.
(39) In all cases, percent conversions refer to HPLC area percent measured at 215 nm. Conversion = (area product)/(area product + area starting material).

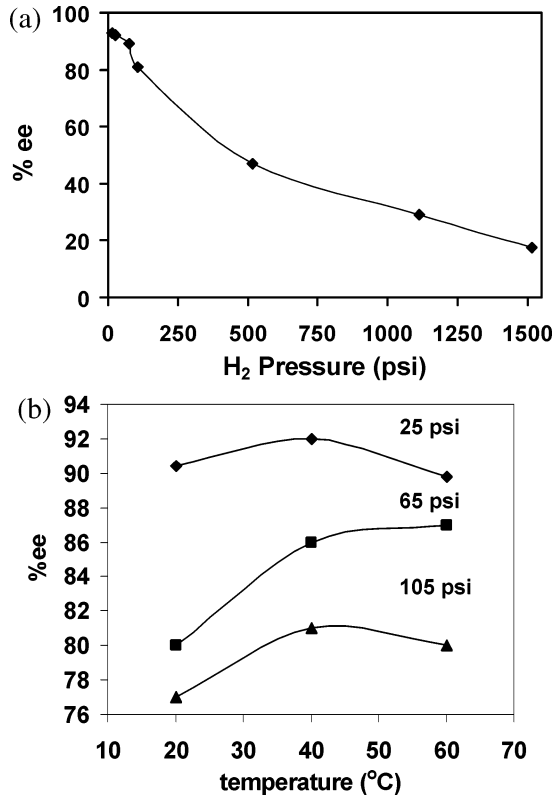

Figure 2. (a) Impact of pressure on enantioselectivity. (b) Impact of temperature and pressure on enantioselectivity of hydrogenation of **1-E·TMG**. Reaction conditions: 0.5 mol % **3**, MeOH, 20 h.

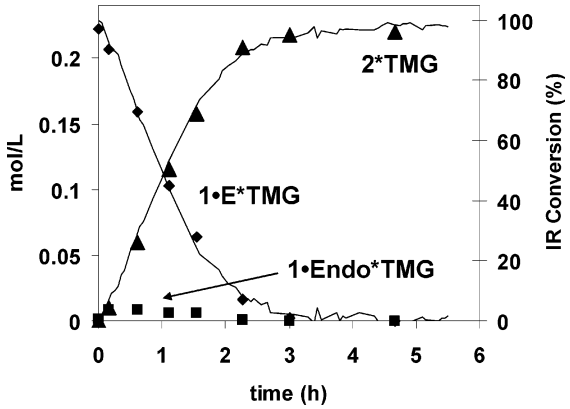

Figure 3. Reaction profile of hydrogenation of **1-E·TMG** (30 psi H_2). The triangles, diamonds, and squares represent HPLC samples (mol/L), and the solid lines represent ReactIR data expressed as a function of conversion (**1-E·TMG**, 1625 cm^{-1}; **2·TMG**, 1588 cm^{-1}).

discovery or mechanism have been limited to simple acyclic model compounds. Prompted by these facts, we decided to further investigate the mechanism of the asymmetric hydrogenation, with the goal of elucidating the origin of the reaction hydrogen pressure dependence.

2. Identification and Characterization of Olefin Isomers of Ene Acid 1. Having successfully demonstrated the hydrogenation reaction, we chose to utilize *in situ* ReactIR, H_2 uptake, and reaction sampling to follow the hydrogenation reaction kinetics and probe for intermediates that might provide insight into the inverse relationship between pressure and enantioselectivity.

A. Synthesis of 1-Endo. A typical hydrogenation reaction profile performed at 30 psi H_2 is illustrated in Figure 3. Greater than 99% conversion was obtained in approximately 5 h, with a good correlation between the hydrogen uptake data, IR data, and HPLC analysis. The enantioselectivity, obtained from periodic reaction sampling, does not change as a function of conversion (90−91% ee). Most importantly, the reaction samples revealed the presence of a new compound, as determined by HPLC. This species, identified as **1-Endo·TMG**, is an endocyclic isomer of **1-E** (see eq 3). It was generated in small quantities during the initial stages of the reaction and consumed to give **2·TMG** prior to reaction completion (vide infra).

For characterization purposes, the endocyclic isomer **1-Endo·TMG** was synthesized in appreciable amounts by heating **1-E·TMG** with catalyst **3** in the absence of hydrogen (eq 3). This process generated a 77:23 equilibrium mixture of **1·TMG**

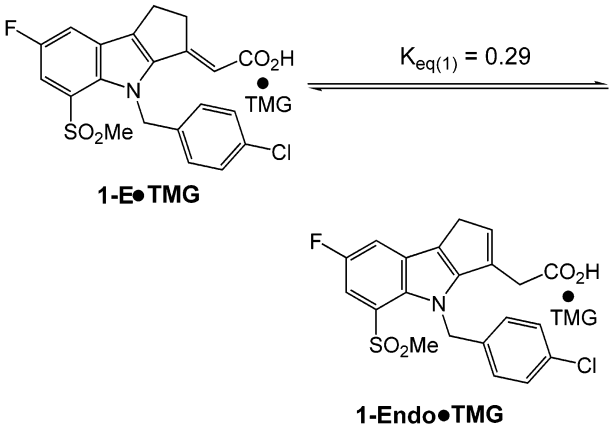

(3)

conditions: ***3*** *(1.2 mol%), MeOH, 3 h, 50 °C*

and **1-Endo·TMG,** respectively ($K_{eq} = 0.29$).[40] The maximum rate of isomerization was determined to be 1.4×10^{-5} mol/L·s and was calculated from data obtained via the periodic sampling of the reaction as it approached equilibrium. The endocyclic isomer was isolated in pure form from this reaction mixture by selective precipitation of **1-E** upon addition of excess acetic acid. Finally, crystals suitable for single-crystal X-ray diffraction analysis were obtained from THF/heptane. The ORTEP diagram can be found in the Supporting Information and provides definitive evidence for the molecular architecture shown in eq 3.

B. Synthesis of 1-Z. We were initially surprised that catalyst **3** isomerized **1-E** to **1-Endo** and not to **1-Z**, the *Z* isomer of **1**. This was due, in part, to the observation made previously in our laboratories that the free indole, which lacked the *N*-BnCl functional group, could be prepared as a 1:1 mixture of *E*/*Z* isomers.[41] In this case, the endo isomer was not observed. Intrigued by this difference, we attempted to prepare the *Z* isomer of **1** by photochemical means. A methanol solution of **1-E·TMG** was exposed to UV light (254 nm), and after 90 min, an equilibrium mixture containing **1-E·TMG** and **1-Z·TMG**

(40) Heating a methanol solution of **1-E·TMG** in the absence of catalyst for 12 h at 50 °C does not produce **1-Endo·TMG**.
(41) Journet, M.; Sarraf, S. Personal communication.

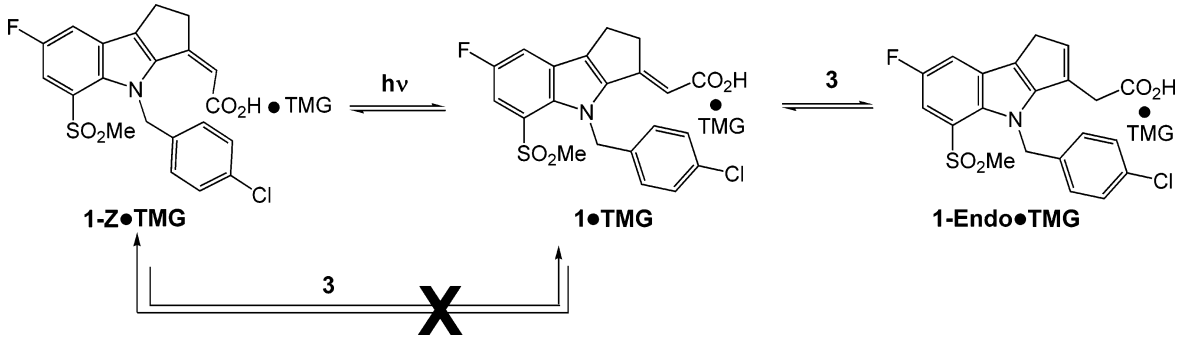

Figure 4. Summary of the thermal and photochemical isomerization behavior observed for **1**.

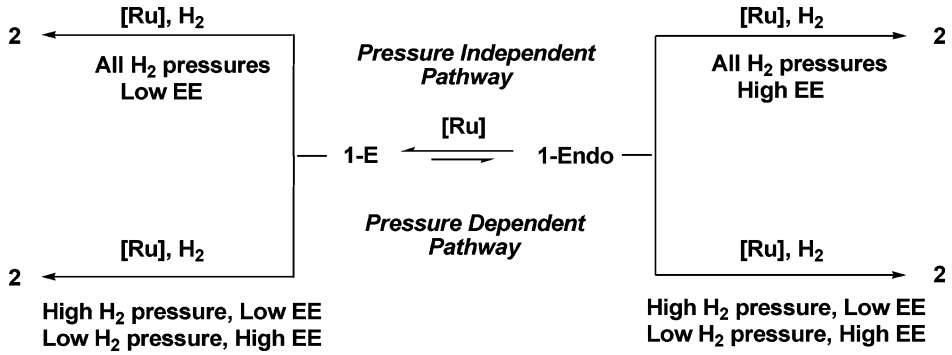

Figure 5. Rationalization of enantioselectivity via pressure-dependent and -independent hydrogenation pathways for **1-E** and **1-Endo**.

(63:37) was observed (eq 4). Prolonged irradiation did not alter this ratio.[42] Compound **1-Endo·TMG** was not formed under

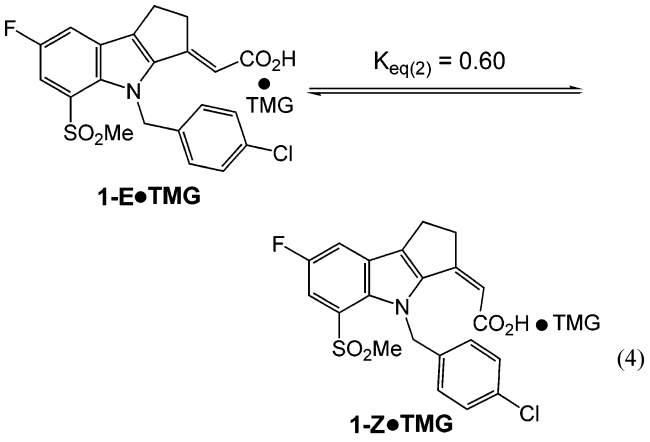

conditions: hν (254 nm), RT, MeOH

these photochemical conditions. The *Z* isomer, **1-Z**, was characterized by HPLC/MS and NMR spectroscopy and was not separated from **1-E**. Of note are the benzyl methylene protons which, by ^{1}H NMR spectroscopy in CD_3CN at 22 °C, exhibit resonances which are nearly broadened into the baseline. These resonances sharpen upon warming the solution to 60 °C. In contrast, the benzyl methylene protons in **1-E·TMG** and **1-Endo·TMG** are sharp at room temperature in the ^{1}H NMR spectrum. The broadened proton signals in the case of **1-Z** are most likely a result of hindered rotation about the nitrogen−benzyl carbon bond of **1-Z**. We attribute this hindered rotation to the fact that the carboxylic acid group is now oriented directly into the benzyl group. For the case of the free indole described above, this steric interaction is absent, so the *Z* olefin geometry is accessible under thermal conditions.

We were interested in ruling out the intermediacy of the *Z* isomer in the hydrogenation reaction pathway. Despite the fact that the *Z* isomer was not observed by HPLC and NMR spectroscopic analysis when **1-E** was heated with **3**, it was difficult to conclusively rule out the formation of very small amounts of this material during the hydrogenation reaction. Catalyst **3** was therefore added to a methanol solution containing a mixture of **1-E** and **1-Z** and heated. After 3 h, by HPLC, a mixture containing the *E*, *Z*, and endo isomers was present. Importantly, the concentration of **1-Z** remained unchanged—the endo isomer was generated exclusively from the *E* isomer. This is represented in Figure 4. Since the concentration of **1-Z** remains constant in the presence of **3**, by the principle of microscopic reversibility, **3** does not catalyze the equilibrium between **1-Z** and **1-E** under thermal conditions. *The lack of isomerization reactivity between **1-Z** and **3** rules out the intermediacy of **1-Z** in the hydrogenation of olefin **1-E**.*

3. Examination of Hydrogen Pressure Dependence of 1-Endo, 1-Z, and 1-E. A. Pressure-Dependent Reaction Mechanisms. We postulated that two limiting mechanisms can be used to rationalize the pressure dependence observed in the hydrogenation of **1-E** (Figure 5). In the first case, the pressure-independent pathway, **1-E** and **1-Endo** are in a ruthenium-catalyzed equilibrium with each other. At all hydrogen pressures, **1-Endo** is hydrogenated by the ruthenium catalyst with high enantioselectivity, and **1-E** is hydrogenated with lower enantioselectivity. In order to achieve the highest enantioselectivity, the reaction must funnel entirely through **1-Endo**. At low pressure, the rate of isomerization is faster than the rate of hydrogenation. This is a Curtin−Hammett-type regime, in that the relative rates of hydrogenation of **1-E** and **1-Endo** dictate enantioselectivity, not the relative rates of isomer interconver-

(42) Photolysis of **1-E·TMG** in CD_3OD does not incorporate deuterium into either **1-E·TMG** or **1-Z·TMG**.

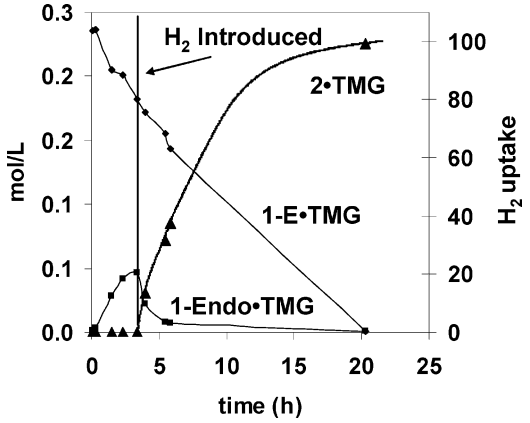

Figure 6. Isomerization and hydrogenation reaction profile of **1-E·TMG**/**1-Endo·TMG** at 25 psi H_2. The diamonds, triangles, and squares represent HPLC samples, and the "X" represents hydrogen uptake. The lines through these symbols serve to better illustrate the reaction profile.

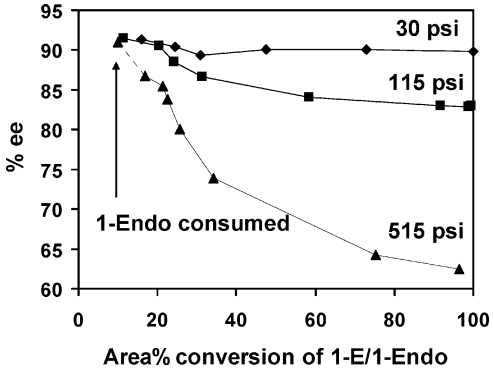

Figure 7. Reaction %ee vs high-performance liquid chromatography (HPLC) area % conversion of the **1-E**/**1-Endo** mixture as a function of H_2 pressures.[49]

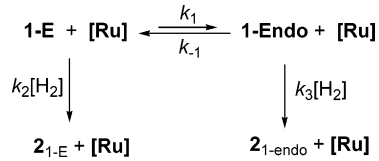

Figure 8. Isomerization and hydrogenation mechanism for **1-E**. Compound $\mathbf{2_{1-E}}$ refers to product derived from **1-E**, and $\mathbf{2_{1-Endo}}$ refers to product derived from **1-Endo**.

sion.[43] Deviation from the Curtin−Hammett regime is observed at high pressures, where the relative rates of hydrogenation and isomerization are competitive. At these high pressures, **1-E** is consumed faster than it can isomerize to **1-Endo**. The second mechanism has **1-E** and **1-Endo** in equilibrium. In this pressure-dependent pathway, both isomers exhibit a negative pressure effect, with higher hydrogen pressures (>25 psi) giving lower enantioselectivities. Pressure effects of this type have been noted previously.[44−47]Alternatively, the overall mechanism can be described as a combination of the hydrogenation pathways illustrated in Figure 5, with one isomer exhibiting a pressure dependence while the other isomer does not. In order to identify which pathway is operational, it was essential to ascertain the hydrogen pressure dependence of each isomer independently.

B. 1-Endo Hydrogenation. An equilibrium mixture of **1-E** and **1-Endo** was prepared by heating **1-E** with **3** for 3 h. This solution was then exposed to 25, 115, and 515 psi H_2.[48] Samples were taken periodically and analyzed by chiral and achiral HPLC. A typical reaction profile is illustrated in Figure 6, and the resulting determination of enantiomeric excess vs conversion is shown in Figure 7. Each reaction is characterized by the rapid initial consumption of **1-Endo**, followed by the relatively slow consumption of **1-E**. These rate differences are consistent with the observation that little endo isomer is observed during hydrogenations of the *E* isomer; i.e., the endo isomer is consumed as soon as it formed. Another striking feature from these data is highlighted in the profile of the reaction enantioselectivity as a function of conversion (Figure 7). As soon as the endo isomer is consumed in the initial stages of the reaction, the reaction enantioselectivity drops substantially until it eventually levels off near reaction completion. From these data, it is clear that *the enantioselectivity of the endo isomer hydrogenation is not influenced by pressure*. The inherent enantioselectivity for the endo isomer is 92% at the pressures examined.

C. 1-E Hydrogenation Kinetics. We next sought to examine the influence of hydrogen pressure on the reaction enantioselectivity for isomer **1-E**. In contrast to **1-Endo**, determination of the inherent enantioselectivity for **1-E** hydrogenation is complicated by the fact that **1-Endo** is in equilibrium with **1-E**. We have shown that **1-Endo** is consumed faster than the **1-E**/**1-Endo** isomerization, and as such, the measured ee from **1-E** hydrogenation is a function of the contribution from both **1-Endo** and **1-E**, as illustrated in Figure 8.

We initially tried to circumvent this problem by performing reactions at elevated H_2 pressures in hopes of identifying a regime wherein the contribution from **1-Endo** was minimized (i.e., $k_2[H_2] \gg k_1$). The results from these experiments are presented in Figure 9a. Nearly zero-order kinetics in **1** are observed over 70% of the reaction (10−80% conversion). The corresponding rate data obtained in this zero-order region are plotted as a function of pressure at a specified conversion in Figure 9b and listed in Table 2. Note that, as hydrogen pressure is increased, a nonlinear increase in reaction rate is observed (Figure 9b). Recall that the maximum rate of isomerization in the absence of hydrogen was found to be 1.5×10^{-5} mol/L·s (see section 2A). Thus, at 33 psi, the isomerization rate and hydrogenation rate are nearly identical, and the rate of hydrogenation ($k_2[H_2]$) at 515 psi (7.5×10^{-5} mol/L·s) is still competitive with the rate of isomerization (k_1, Table 2).

Despite the inability to reach a limiting regime where isomerization did not compete with hydrogenation, the inherent enantioselectivity for **1-E** reduction at different hydrogen pressures could be approximated using the hydrogenation rate data at different pressures. In order to do this, two approximations were made: (1) the isomerization rate is constant regardless of hydrogen pressure and (2) **1-Endo** is consumed immediately

(43) Carey, F. A.; Sundberg, R. J. *Advanced Organic Chemistry, Part A: Structure and Mechanisms*; Plenum: New York, 1993.
(44) Landis, C. R.; Halpern, J. *J. Am. Chem. Soc.* **1987**, *109*, 1746−1754.
(45) Yoshikawa, K.; Murata, M.; Yamamoto, N.; Inoguchi, K.; Achiawa, K. *Chem. Pharm. Bull.* **1992**, *40*, 1072−1074.
(46) Saburi, M.; Takeuchi, H.; Ogasawara, M.; Tsukahara, T.; Ishii, Y.; Ikariya, T.; Takahashi, T.; Uchida, Y. *J. Organomet. Chem.* **1992**, *428*, 155−167.
(47) Daley, C. J. A.; Wiles, J. A.; Bergens, S. H. *Can. J. Chem.* **1998**, *76*, 1447−1456.
(48) Solutions of pure **1-Endo** in the presence of catalyst isomerize to generate an equilibrium mixture with **1-E**. As such, we opted to start with the equilibrated mixture instead of pure **1-Endo** to ensure that the starting concentration of **1-Endo** was constant between experiments. Consistent with results from Figure 7, the high-pressure syringe pump addition of catalyst to a solution of **1-Endo** at 100 psig H_2 and 50 °C produced **2** in 92% ee.
(49) At 515 psi, the reaction rate was sufficiently fast that complete consumption of **1-Endo** isomer and some of the **1-E** isomer had occurred at 20 area % conversion. The point at 10 area % conversion at 515 psi is calculated by removing the contribution from **1-E**.

Table 2. Rate Data and %ee for the Hydrogenation of **1-E** at Different Hydrogen Pressures

hydrogen pressure (psi)	rate (mol/L·s)	$\%ee_{total}$ (measured)[b]	$\%ee_{1-E}$ (calculated)
0	1.4×10^{-5} [a]	na	na
33	1.5×10^{-5}	91	63
115	4.8×10^{-5}	80	74
515	7.5×10^{-5}	47	36

[a] Isomerization rate (r_{isom}), see section 2A. [b] Enantiomeric excesses were measured at 100% conversion.

after it is generated; therefore, hydrogenation of **1-Endo** is only as fast as the rate of isomerization from **1-E** to **1-Endo**. The first approximation assumes that the isomerization catalyst is the same at all pressures examined. This is supported by the fact that solutions exposed to hydrogen for 0, 15, 30, and 60 min exhibit near identical isomerization rates.[50] The second assumption relies on the fact that **1-Endo** does not build up during the hydrogenation reactions. This is demonstrated by independent studies where **1-Endo** is consumed substantially faster than **1-E** (Figure 6).

Using the approximations described above, the overall reaction enantioselectivity ($\%ee_{total}$) of the hydrogenation can be expressed as a contribution from both **1-E** and **1-Endo** (eq 5).[51] This contribution is defined by the relative rates of hydrogenation of **1-E** and **1-Endo**, noted as $r_{\mathbf{1-E}}$ and $r_{\mathbf{1-Endo}}$, respectively. The rate of **1-Endo** hydrogenation ($r_{\mathbf{1-Endo}}$) is substituted with the rate of isomerization (r_{isom}) since the rate of endo hydrogenation is limited by the rate at which **1-E** isomerizes to **1-Endo** (eq 6). Rearranging eq 6 in terms of $\%ee_{\mathbf{1-E}}$ yields eq 7.

$$\%ee_{total} = \left(\frac{r_{\mathbf{1-E}}}{r_{\mathbf{1-E}} + r_{\mathbf{1-Endo}}}\right)\%ee_{\mathbf{1-E}} + \left(\frac{r_{\mathbf{1-Endo}}}{r_{\mathbf{1-E}} + r_{\mathbf{1-Endo}}}\right)\%ee_{\mathbf{1-Endo}} \quad (5)$$

$$\%ee_{total} = \left(\frac{r_{\mathbf{1-E}}}{r_{\mathbf{1-E}} + r_{1-isom}}\right)\%ee_{\mathbf{1-E}} + \left(\frac{r_{isom}}{r_{\mathbf{1-E}} + r_{isom}}\right)\%ee_{\mathbf{1-Endo}} \quad (6)$$

$$\%ee_{\mathbf{1-E}} = \left[\%ee_{total} - \left(\frac{r_{isom}}{r_{\mathbf{1-E}} + r_{isom}}\right)\%ee_{\mathbf{1-Endo}}\right] \Big/ \left(\frac{r_{\mathbf{1-E}}}{r_{\mathbf{1-E}} + r_{\mathbf{1-Endo}}}\right) \quad (7)$$

With eq 7, the data in Table 2, and the inherent enantioselectivity for **1-Endo** ($\%ee_{\mathbf{1-Endo}} = 92$, see section 3B), the inherent enantioselectivity of the *E* isomer (**1-E**) can be calculated at different hydrogen pressures. The results, shown in the last column of Table 2, reveal that *the inherent enantioselectivity of the **1-E** isomer hydrogenation is a function of hydrogen pressure.* In particular, the enantioselectivity exhibits negative pressure dependence, with %ee decreasing as hydrogen pressure increases. This is most clearly illustrated at 115 and 515 psi, where the calculated ee for **1-E** drops from 74% to 36% as the hydrogen pressure is increased. At 33 psi, the reaction rate and isomerization rate are nearly identical; as a result, it is difficult to accurately calculate the %ee for **1-E**, as its final contribution to the overall ee is negligible (<7%).

(50) This information can be found in the Supporting Information.
(51) An identical result is obtained when the relative ratios of the *R* and *S* enantiomers are used in place of %ee.

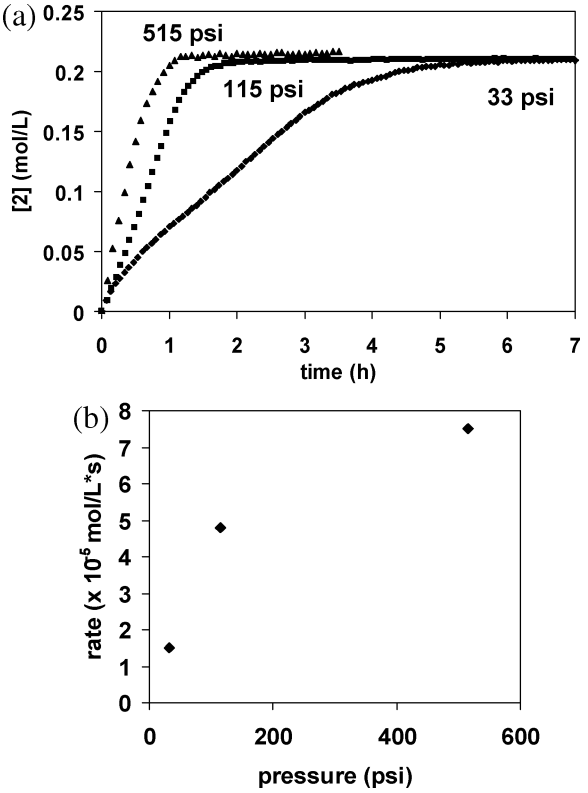

Figure 9. (a) Kinetic profile of the reaction of **1-E** with **3** at different hydrogen pressures, as monitored by ReactIR. (b) Zero-order rate data plotted as a function of hydrogen pressure at 50% conversion.

Table 3. Hydrogenation of **1-E·TMG**/**1-Z·TMG** Mixture at Two Different H_2 Pressures with **3** (1.2 mol %), Comparison with Pure **1-E·TMG**, and Calculation of Inherent Enantioselectivity of **1-Z**

entry	H_2 pressure (psi)	%**1-E**	%**1-Z**	%ee (measured)	$\%ee_{1-Z}$ (calculated)
1	25	62	37	59	5
2	25	100	0	91	na
3	105	62	37	46	−13
4	105	100	0	82	na

At elevated pressures (>100 psi), the rate of hydrogenation of **1-E** is faster than the rate of isomerization to **1-Endo**; consequently, the contribution of **1-E** to the overall ee is substantial. As noted above, these calculations rely upon the assumption that the rate of isomerization is independent of hydrogen pressure. While this phenomenom cannot be experimentally verified, additional support for this pressure-dependent mechanism was determined for **1-Z**, where complications arising from **1-Endo** are nonexistent (vide infra).

D. 1-Z Hydrogenation. While the *Z* isomer (**1-Z**) is only accessible via photochemical means, we were still interested in examining its ee pressure dependence with hydrogenation catalyst **3**. After photolysis of **1-E·TMG**, the resulting **1-E·TMG**/**1-Z·TMG** mixture (62:37) was added to a solution containing catalyst **3** and placed under H_2 at 25 and 105 psi. Greater than 95 area % conversion of both the *E* and *Z* isomers was obtained.[52] The enantioselectivities at each pressure, along with a comparison of the hydrogenation of pure **1-E**, are shown in Table 3. Since **1-E** and **1-Z** do not interconvert under thermal conditions, the inherent enantiomeric excess for the hydrogena-

(52) Qualitatively, the *Z* isomer was less reactive than the *E* isomer toward hydrogenation with **3**.

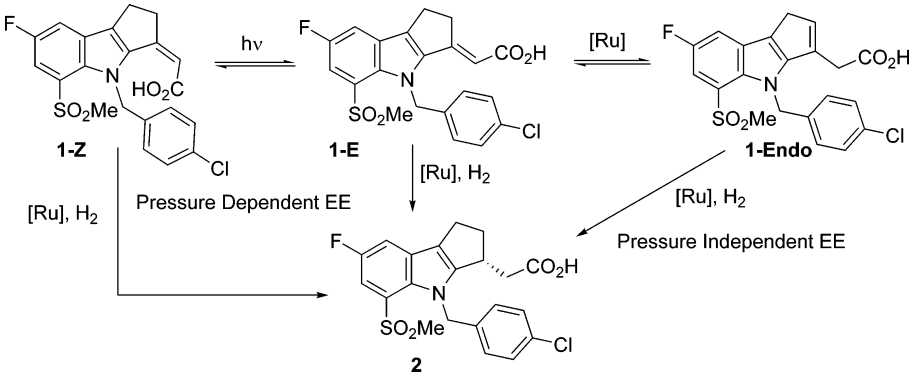

Figure 10. Proposed hydrogen dependence for isomers **1-E**, **1-Z**, and **1-Endo**.

tion of the *Z* isomer at both pressures can be calculated. The overall reaction enantioselectivity (%ee$_{total}$) is a function of both the *E* and *Z* contributions (eq 8). Since the %ee of **1-E** (%ee$_{\mathbf{1-E}}$) can be measured independently, the inherent enantioselectivity of **1-Z** can therefore be measured by rearranging eq 8 in terms of %ee$_{\mathbf{1-Z}}$, to give eq 9.[51]

$$\%ee_{total} = (\%\mathbf{1\text{-}E} \times \%ee_{\mathbf{1-E}}) + (\%\mathbf{1\text{-}Z} \times \%ee_{\mathbf{1-Z}}) \quad (8)$$

$$\%ee_{\mathbf{1-Z}} = \frac{\%ee_{total} - (\%\mathbf{1\text{-}E} \times \%ee_{\mathbf{1-E}})}{\%\mathbf{1\text{-}Z}} \quad (9)$$

With eq 9, the *Z* isomer's hydrogenation enantioselectivity was determined at different pressures (Table 3, column 6). Upon increasing the pressure from 25 to 105 psi, the reaction enantioselectivity changes from +5% ee to −13% ee. Analogous to α,β-unsaturated acid **1-E**, *the inherent enantioselectivity of the hydrogenation of the Z-isomer is a function of hydrogen pressure*. Figure 10 summarizes the hydrogen pressure-dependent behavior of isomers **1-E**, **1-Endo**, and **1-Z**.

E. Remarks on the Pressure-Dependent Hydrogenation Mechanism of 1-E. Rationales for pressure effects in hydrogenation reactions have been proposd previously. Work by Achiawa and co-workers described the hydrogenation of tiglic acid at low and high pressures with (BIMOP)Ru(OAc)$_2$, a catalyst employing an axially chiral ligand similar to BINAP. It was found that the enantioselectivity of tiglic acid hydrogenation did vary with pressure, with lower pressures giving higher enantioselectivities.[45] To rationalize this, the authors proposed a mechanism whereby the rates of hydrogenation of the diastereomeric ruthenium−tiglic acid complexes dictated enantioselectivity. This mechanism is analogous to that invoked by Halpern and Landis for dehydroamino acids and can be applied to **1-E**.[44] In particular, the reaction enantioselectivity is set by the relative rates of ruthenium−substrate diastereomer interconversion and their subsequent hydrogenation. Further elucidation of this mechanism for **1-E** will necessitate identification of intermediates via direct spectropic evidence and kinetic decoupling from the **1-Endo** pathway.

4. Elucidation of 1-Endo Hydrogenation Mechanism via Deuterium Labeling Studies. There are few reported examples of asymmetric β,γ-unsaturated olefin hydrogenations.[29,46,53−56] This is likely because the corresponding α,β isomer is typically more stable due to conjugation of the olefin and carboxylic acid π orbitals. We therefore saw this as a unique opportunity to gain further insight into the mechanism of **1-Endo** hydrogenation via use of deuterium labeling studies.

Compound **1-Endo** was treated with **3** and D_2 in CH_3OH (eq 10). Notably, this reduction is both regioselective and

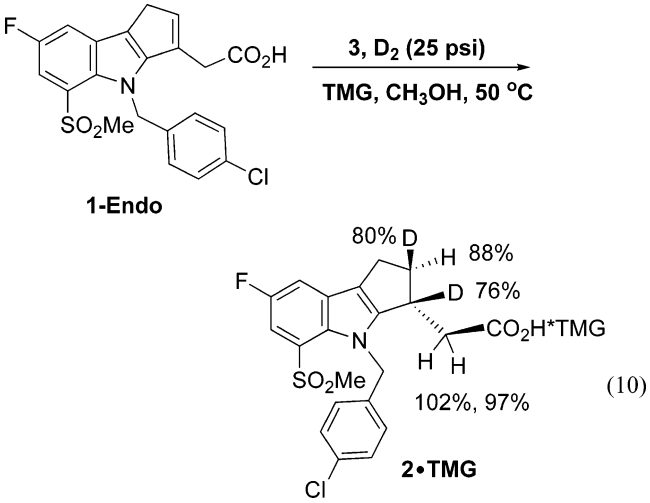

(10)

diastereoselective, with deuterium formally adding in a cis fashion across the double bond of **1-Endo**. Relatively little hydrogen from the solvent is incorporated into **2**. The location of deuterium observed in hydrogenation of **1-Endo** was somewhat surprising in light of the fact that hydrogenation of tiglic acid and related substrates with (BINAP)Ru(OAc)$_2$, a catalyst similar to **3**, results in the incorporation of one hydrogen atom and one deuterium atom.[57−59] In this case, it was postulated that, following olefin insertion into the Ru−D bond, the resulting metal carbon bond is cleaved by a proton from the solvent. For tiglic acid, the reaction is performed under neutral conditions, i.e., in the absence of added base as is the case with **1-Endo**. We therefore decided to explore the impact of base on the hydrogenation of both **1-Endo** and tiglic acid with (BINAP)-Ru(OAc)$_2$.[60] It is stressed that hydrogenation of both **1-E** and **1-Endo** with either catalyst **3** or (BINAP)Ru(OAc)$_2$ gives **2** with identical enantioselectivity.

(53) Bulliard, M.; Laboue, B.; Lastennet, J.; Roussiasse *Org. Process Res. Dev.* **2001**, *5*, 438−441.
(54) Burk, M. J.; Bienewald, F.; Challenger, S.; Derrick, A.; Ramsden, J. A. *J. Org. Chem.* **1999**, *64*, 3290−3298.
(55) Boulton, L. T.; Lennon, I. C.; McCague, R. *Org. Biomol. Chem.* **2003**, *1*, 1094−1096.
(56) Yamamoto, K.; Ikeda, K.; Yin, L. K. *J. Organomet. Chem.* **1989**, *370*, 319−332.
(57) Ashby, M. T.; Halpern, J. *J. Am. Chem. Soc.* **1991**, *113*, 589−594.
(58) Ager, D. J.; Babler, S.; Froen, D. E.; Laneman, S. A.; Pantaleone, D. P.; Prakash, I.; Zhi, B. *Org. Process Res. Dev.* **2003**, *7*, 369−378.
(59) Ohta, T.; Takaya, H. *Tetrahedron Lett.* **1990**, *31*, 7189−7192.

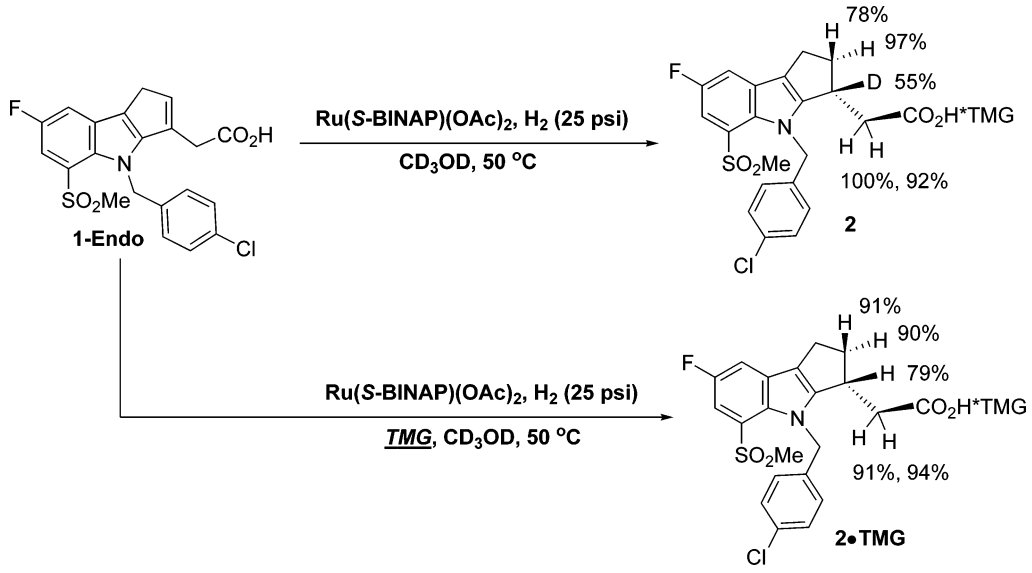

Figure 11. ^{1}H NMR spectroscopic results from the hydrogenation of **1-Endo** with and without added TMG, catalyzed by Ru(*S*-BINAP)(OAc)$_2$.

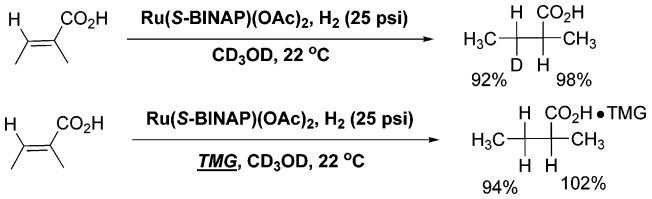

Figure 12. ^{1}H NMR spectroscopic results from the hydrogenation of tiglic acid with and without added TMG, catalyzed by Ru(*S*-BINAP)(OAc)$_2$.

As illustrated in Figure 11, **1-Endo** was treated with Ru(*S*-BINAP)(OAc)$_2$ (5 mol %) and H_2 in CD_3OD with and without TMG. Markedly different deuterium incorporation patterns are seen in these two reactions.[61] When the hydrogenation is performed with TMG, results similar to those observed in eq 10 are obtained; namely, hydrogen incorporation is predominantly seen in both the β and γ positions. In contrast, the hydrogenation in the absence of base results in the incorporation of hydrogen in the γ position and deuterium in the β position, similar to the reports with tiglic acid. As noted by others, H/D exchange between hydrogen gas and alcoholic solvents by this class of ruthenium catalysts is rapid.[10,46,57,59,62] As such, the results illustrated in Figure 11 for the reaction run in the absence of TMG are complicated by this exchange. Nonetheless, this result suggests that, for **1-Endo**, ruthenium is placed in the β position, not the γ position, following insertion (vide infra). Under basic conditions, reaction with hydrogen, not solvent, liberates the product.

In order to ascertain whether this observation with **1-Endo**, a β,γ-unsaturated acid, was pertinent to tiglic acid, an α,β-unsaturated acid, we attempted the tiglic acid hydrogenation with Ru(*S*-BINAP)(OAc)$_2$ with and without TMG (Figure 12). As described by Ashby and Halpern, under "neutral" conditions, hydrogen incorporation is observed in the α position and deuterium incorporation is observed in the β position.[57] Gratifyingly, the presence of base does indeed have an impact on the H/D incorporation pattern. In the presence of TMG (1 equiv), the H/D incorporation pattern changes, with hydrogen incorporation dominant in *both* the α and β positions. These results suggest that, under basic conditions, hydrogenolysis, *not* protonolysis, is the primary mode of metal−carbon bond cleavage.[63,64]

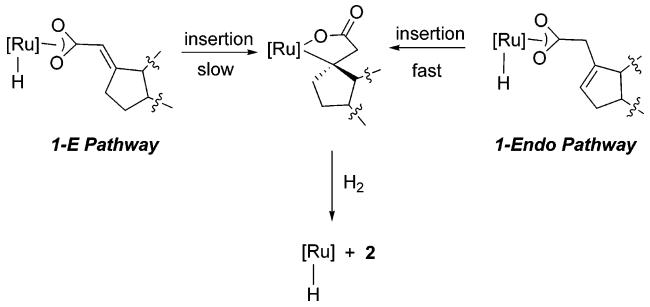

Figure 13. Postulated mechanism for hydride insertion and hydrogenolysis for **1-E** and **1-Endo**.

On the basis of the results from the labeling studies of **1-Endo** and tiglic acid, a more detailed mechanistic picture for the hydrogenation of **1-E** and **1-Endo** under basic conditions can be discerned. The insertion and reductive elimination steps for **1-E** and **1-Endo** are shown in Figure 13.[65] For the *E* isomer, which is analogous to tiglic acid, Ru−H insertion places the ruthenium in the β position, creating a five-member chelate.[57,62,64] Hydrogenolysis liberates **2** and regenerates the catalyst. For **1-Endo**, Ru−H insertion places the ruthenium in the β position, to produce the same intermediate proposed for **1-E** hydrogenation. Subsequent hydrogenolysis liberates **2**.

Despite the fact that **1-E** and **1-Endo** produce the same intermediate after insertion, the hydrogenation rate *and* enantioselectivity for these two compounds are markedly different (vide supra). This is attributed to a difference in energy between

(60) The acetate catalyst, Ru(*S*-BINAP)OAc$_2$, was employed because catalyst **3** does not react with the free acid. It is thought that base is required to facilitate cymene displacement and generation of the active catalyst.
(61) The reaction enantioselectivity with (*S*-BINAP)Ru(OAc)$_2$ with and without TMG was 92−93.%.
(62) Daley, C. J. A.; Wiles, J. A.; Bergens, S. H. *Inorg. Chim. Acta* **2006**, *359*, 2760−2770.
(63) A similar observation was noted by Chan and co-workers in the hydrogenation of a naproxen precursor with a ruthenium catalyst under basic conditions. See ref 64.
(64) Chan, A. S. C.; Chen, C. C.; Yang, T. K.; Huang, J. H.; Lin, Y. C. *Inorg. Chim. Acta* **1995**, *234*, 95−100.
(65) The substrate is assumed to be bound to the metal via the carboxylate linkage. This is supported by literature reports (see ref 57 and 66) and the observation that the methyl ester derivative of **1** is not hydrogenated by **3**.

the two insertion steps. We postulate that rearrangement to the geometry necessary for insertion is more facile for the β,γ-substituted olefin **1-Endo**, as it is not locked in as rigid a conformation as α,β-substituted olefin **1-E**. The difference in enantioselectivity can be attributed to the fact that **1-Endo** can coordinate to the metal by both the carboxylate and olefin groups. The ruthenium-**1-Endo** intermediate is analogous to the rhodium−acetamidocinnamate described by Landis and Halpern.[44] This binding mode should offer more stereodifferentation than the ruthenium-**1-E** intermediate, where only the carboxylate group can bind to the metal.[57,66,67]

Summary and Conclusions

This work describes the implementation of an asymmetric hydrogenation of a pharmaceutically relevant compound. It is clear from this example that, despite the increased substrate complexity, asymmetric hydrogenation can be a practical industrial tool. Surprisingly, this work represents a rare example of a mechanistic study on an asymmetric hydrogenation of industrial relevance.[54] It is exactly a result of the increased substrate complexity that new mechanistic challenges and opportunities, not available with structurally less diverse substrates, become available.

Experimental Section

Materials. Unless otherwise noted, reagents were purchased from commercial suppliers and used without further purification. All NMR spectra were recorded at room temperature unless otherwise noted. Compounds **1-E**,[26] **2**,[16] **2-Br**,[18] and Ru(*S*-BINAP)$(OAc)_2$[68] were prepared according to literature procedures. Resealable pressure vessels were purchased from Andrews Glass Co., and the Multimax IR instrument was purchased from Mettler-Toledo.

Preparation of Catalyst 3. A modified version of a literature procedure was followed.[32] In an inert atmosphere glovebox, degassed methanol (75 mL) was charged to a round-bottom flask containing [(*p*-cymene)$RuCl_2$]$_2$ (0.37 g, 0.60 mmol), (*S*)-BINAP (0.77 g, 1.2 mmol), and a stir bar. Degassed toluene (25 mL) was added, and the orange heterogeneous solution was transferred to an ampule with a resealable Kontes adapter. The ampule was sealed, removed from the glovebox, and heated for 1−2 h at 50−60 °C with stirring. The clear, orange solution was brought into a glovebox and stored at room temperature as a stock solution (approximate molarity = 0.012).

Typical Catalyst Screening Protocol. Solid substrate (0.023 mmol) was weighed into an HPLC vial (2 mL) containing a stir bar. A total of 14 HPLC vials containing substrate were brought into a glovebox and charged with degassed methanol (180 μL) and triethylamine (0.023 mmol). To the vials was added the appropriate catalyst solution (0.0023 mmol in 20 μL of MeOH/toluene). The HPLC vials were fitted with perforated septa caps and transferred to a resealable pressure vessel (purchased from Andrews Glass Co.) containing sand. The sand was used as the heat-transfer medium and as a means of preventing the vials from tipping over. The vessel was sealed, removed from the glovebox, placed in an oil bath, and attached to a hydrogen/N_2/vacuum manifold. After the solutions were set to stirring and the oil bath was warmed to 50 °C, the vessel was pressurized to 105 psi with N_2 and then vented to atmospheric pressure. This was repeated three times, after which the vessel was pressurized with H_2 (105 psi). After an overnight age, the vessel was vented to atmospheric pressure, and the reaction solutions were analyzed by HPLC or SFC.

Crystallization of 1,1,3,3-Tetramethylguanidinium (2*E*)-[4-(4-Chlorobenzyl)-7-fluoro-5-(methylsulfonyl)-1,4-dihydrocyclopenta-[*b*]indol-3(2*H*)-ylidene]acetate (1-E·TMG). 1,1,3,3-Tetramethylguanidine (TMG, 99%, 25.0 mL, 193 mmol) was charged to a slurry of compound **1-E** (70 g, 160 mmol) in isopropylacetate (IPAc, 280 mL) and MeOH (140 mL) at 23 °C, whereupon the solids dissolved. Additional IPAc (125 mL) was added with previously generated seed, resulting in the formation of a slurry. Additional IPAc (125 mL) was added and the mixture stirred overnight. The slurry was distilled at constant volume by the simultaneous addition of IPAc. When the supernatant reached 5 mg/mL, distillation was discontinued and the slurry cooled in an ice bath. The crystals were filtered and washed with ice-cold IPAc. Drying yielded 86.0 g of crystalline solid of 96.8 wt % purity. ^{1}H NMR (400 MHz, CD_3OD): δ 6.87 (dd, 1H, J_{HH} = 9.6 Hz, J_{HF} = 2.7 Hz), 6.76 (dd, 1H, J_{HH} = 7.9 Hz, J_{HF} = 2.7 Hz), 6.43 (d, 2H, J_{HH} = 8.5 Hz), 6.06 (d, 2H, J_{HH} = 8.5 Hz), 5.36 (s, 2H), 5.21 (t, J_{HH} = 2.2 Hz), 2.79 (bm, 2H, J_{HH} = 3.2 Hz), 2.16 (s, 3H), 2.14 (s, 15H), 2.10 (bm, 2H). $^{13}C\{^1H\}$ NMR (101 MHz, CD_3OD): δ 175.9 (s), 163.3 (s), 157.1 (d, J = 239 Hz), 148.8 (s), 145.5 (s), 138.9 (s), 136.4 (s), 134.0 (s), 133.5 (d, J = 5 Hz), 130.0 (s), 129.8 (d, J = 8.8 Hz), 128.6 (s), 127.9 (d, J = 7 Hz), 118.1 (s), 115.6 (s), 115.3 (s), 112.5 (s), 112.3 (s), 51.1 (s), 45.1 (s), 40.1 (s), 37.0 (s), 23.4 (s).

(2*E*)-[5-Bromo-4-(4-chlorobenzyl)-7-fluoro-1,4-dihydrocyclopenta-[*b*]indol-3(2*H*)-ylidene]acetic Acid (1-Br-E). To a solution of [4-(4-chlorobenzyl)-7-fluoro-5-bromo-1,2,3,4-tetrahydrocyclopenta[*b*]indol-3-yl]acetic acid (**2-Br**, 44.0 g, 0.10 mol) in toluene (450 mL) was added *N*-chlorosuccinimide (16.0 g, 0.12 mol) portionwise over 5 min. The resulting solution was stirred at room temperature for 1 h, after which acetic acid (11.5 mL, 0.20 mol) was added. The reaction mixture was stirred for an additional 2 h at 22 °C to crystallize the product. The slurry was filtered, rinsed with toluene (150 mL), and dried at 40 °C under vacuum for 24 h to give 40.4 g of the ene acid (93%) as the pure *E* isomer. Due to its limited solubility, compound **1-Br-E** was characterized spectroscopically as the TMG salt, **1-Br-E·TMG**. ^{1}H NMR (400 MHz, CD_3OD): δ 7.25 (d, 2H, J_{HH} = 8.4 Hz), 7.17 (dd, 1H, J_{HH} = 8.4 Hz, J_{HH} = 2.0 Hz), 7.15 (dd, 1H, J_{HH} = 8.4 Hz, J_{HH} = 2 Hz), 6.96 (d, 2H, J_{HH} = 8.4 Hz), 5.98 (s, 1H), 5.89 (s, 1H), 3.60 (bs, 2H), 2.95 (s, 12H), 2.79 (t, 2H, J_{HH} = 5 Hz). $^{13}C\{^1H\}$ NMR (101 MHz, CD_3OD): δ 174.8 (s), 161.8 (s), 158.0 (s), 155.6 (s), 146.3 (s), 144.7 (s), 137.7 (s), 136.2 (s), 132.4 (s), 130.8 (d, J_{CF} = 4.8 Hz), 128.3 (s), 127.2 (s), 126.5 (d, J_{CF} = 10.4 Hz), 116.3 (d, J_{CF} = 29 Hz), 115.6 (s), 103.8 (d, J_{CF} = 23 Hz), 102.7 (d, J_{CF} = 12 Hz), 38.5 (s), 35.6 (s), 22.0 (s). HPLC/MS: m/z for $[C_{20}H_{14}BrClFNO_2]^+$ ($M + H^+$) calcd 433.9959, obsd 433.9957.

[4-(4-Chlorobenzyl)-7-fluoro-5-(methylsulfonyl)-1,4-dihydrocyclopenta[*b*]indol-3-yl]acetic Acid (1-Endo). To a stirred slurry of **1-E** (50.0 g, 0.12 mol) in MeOH (400 mL) was added TMG (13.0 g, 0.12 mol). A stream of nitrogen gas was bubbled into the homogeneous red solution for 15 min to remove residual oxygen, upon which Ru(*S*-BINAP)(*p*-cymene)Cl_2 (120 mL, 0.012 M, 1.2 mol %) was added. The solution was warmed to 50 °C and stirred for 6 h. After the solution cooled to room temperature, an isopropyl acetate (25 mL) solution of acetic acid (7.3 mL, 1.1 equiv, 0.13 mol) was added over 45 min via addition funnel in order to precipitate **1-E**. The solution was stirred an additional hour and then filtered through a frit. The solvent was removed under reduced pressure, and the residual oil was redissolved in EtOAc (250 mL). This solution was washed with 0.1 N HCl (175 mL), water (150 mL), and brine (100 mL) and then transferred to a round-bottom flask containing Darco (3 g of Darco KB, 3 g of Darco G-60) and silica gel (3 g). The Darco and silica gel treatment was employed in order to remove residual ruthenium. After this slurry was agitated for 30 min, the solution was filtered through a medium frit and the solvent removed under reduced pressure. To the resulting foam was added EtOAc (50 mL). Upon this solution being cooled to 0 °C, a white solid

(66) Ashby, M. T.; Khan, M. A.; Halpern, J. *Organometallics* **1991**, *10*, 2011−2015.
(67) A reviewer is acknowledged for suggesting this two-point binding mechanism to rationalize the higher enantioselectivity.
(68) Kitamura, M.; Tokunaga, M.; Noyori, R. *J. Org. Chem.* **1992**, *57*, 4053−4054.

precipitated. This was collected on a filter frit, rinsed with additional ethyl acetate (0 °C, 2 × 10 mL), and dried overnight under reduced pressure (4.30 g, 8.6% yield from **1-E**). ^{1}H NMR (400 MHz, DMSO-d_6): δ 12.61 (s, 1H, CO_2H), 7.79 (dd, 1H, J_{HH} = 8 Hz, J_{HF} = 2 Hz), 7.52 (dd, 1H, J_{HH} = 10 Hz, J_{HF} = 3 Hz), 7.33 (d, 2H, J_{HH} = 8.4 Hz), 6.71 (d, 2H, J_{HH} = 8 Hz), 6.28 (s, 1H), 6.11 (s, 2H), 3.35 (s, 2 H), 3.28 (s, 2 H), 3.20 (s, 3H). ^{13}C{^{1}H} NMR (101 MHz, DMSO-d_6): δ 171.9 (s), 155.2 (d, J_{CF} = 237 Hz), 152.3 (s), 138.2 (d, 25 Hz), 131.7 (d, 7 Hz), 130.4 (s), 128.8 (s), 127.8 (d, 10 Hz), 126.7 (s), 126.6 (d, J = 8 Hz), 122.4 (d, J = 5 Hz), 110.2 (s), 109.9 (s), 109.6 (s), 109.4 (s), 49.3 (s), 44.0 (s), 33.7 (s), 30.9 (s). HPLC/MS: m/z for $[C_{21}H_{16}ClFNO_4S]^+$ (M + H$^+$) calcd 434.0629, obsd 434.0628.

1,1,3,3-Tetramethylguanidinium (2*Z*)-[4-(4-Chlorobenzyl)-7-fluoro-5-(methylsulfonyl)-1,4-dihydrocyclopenta[*b*]indol-3(2*H*)-ylidene]-acetate (1-Z·TMG). A quartz tube was charged with **1-E·TMG** (100 mg, 0.23 mmol) and methanol (5 mL) and placed inside a Rayonet photochemical reactor. At room temperature, the homogeneous solution was exposed to UV radiation (254 nm) for 90 min. The solution was removed from the reactor and analyzed by HPLC. At 215 nm, $K_{eq(2)}$ was determined to be 0.60. The isomers were not separated, and NMR spectra were recorded on the mixture. ^{1}H NMR (400 MHz, CD_3OD): δ 7.61 (dd, 1H, J_{HH} = 8.0 Hz, J_{HH} = 2.7 Hz), 7.49 (dd, 1H, J_{HH} = 8.0 Hz, J_{HH} = 2.7 Hz), 7.04 (d, 2H, J_{HH} = 8.5 Hz), 6.72 (d, 2H, J_{HH} = 8.5 Hz), 5.88 (bs, 1H), 2.96 (s, 12 H). ^{13}C{^{1}H} NMR (101 MHz, $CDCl_3$): δ 176.1 (s), 158.0 (d, J_{CF} = 240 Hz), 151.3 (s), 140.29 (s), 139.11 (s), 138.44 (s), 135.4 (s), 134.2 (s), 131.7 (d, J_{CF} = 9 Hz), 129.6 (s), 129.3 (s), 129.0 (d, J_{CF} = 8 Hz), 119.7 (s), 114.3 (d, J_{CF} = 29 Hz), 112.0 (d, J_{CF} = 23 Hz), 53.2 (s), 50.0 (s), 44.3 (s), 40.8 (s), 23.7 (s).

Hydrogenation Protocol Employing in Situ-Generated 1-E·TMG. ***CAUTION!*** *Hydrogen gas is flammable. Appropriate precautions should be exercised.* To accelerate processing, the TMG salt of **1-E** was prepared in situ by addition of TMG to ene acid **1-E**. As a result, a catalyst loading of 1.2 mol % was employed to ensure >99.9 HPLC area % conversion in 15 h.[69] The hydrogenation was complete (>99.9% conversion) in <10 h, and **2·TMG** was produced in 95% assay yield and 92% ee. A reaction pressure vessel equipped with an overhead stirred was charged with a methanol (9.2 L) slurry of **1-E** (1200 g, 2.8 mol). The slurry was set stirring, and TMG (320 g, 2.8 mmol) was added. The resulting purple/brown slurry was degassed (5 × vacuum/nitrogen), and the ruthenium catalyst, [(*p*-cymene)(*S*-BINAP)RuCl$_2$]$_2$ (2.8 L, 0.012 M in methanol/toluene (3:1), 1.2 mol %), was charged to the vessel. After the lines leading up to the pressure vessel were degassed (5 × vacuum/nitrogen), the stirred solution in the pressure vessel was degassed (3 × nitrogen/vacuum) and pressure purged with hydrogen gas (3 × hydrogen 40 psig/vacuum). The reaction solution was then placed under hydrogen gas (10 psig) and warmed to 45−50 °C. After an overnight age (~15 h), the resulting solution was cooled to room temperature and the pressure vessel vented to atmospheric pressure. The reaction was determined to be complete by HPLC (>99.9 area % conversion, 215 nm). Assay yield = 96% (1.16 kg **2**); % ee = 91. Subsequent downstream processing of **2·TMG** proceeded as expected, producing **2** in high chemical and optical purity.[26]

Hydrogenation Protocol Employing Crystallized 1-E·TMG. ***CAUTION!*** *Hydrogen gas is flammable. Appropriate precautions should be exercised.* In a glovebox, a reaction pressure vessel was charged with **1-E·TMG** (2.5 g, 4.6 mmol), degassed MeOH (25 mL), [(*p*-cymene)(*S*-BINAP)RuCl$_2$]$_2$ (1.9 mL, 0.023 mmol), and a stir bar. The vessel was sealed, removed from the glovebox, and attached to a hydrogen/nitrogen/vacuum manifold. After the lines leading up to the pressure vessel were degassed (5 × vacuum/nitrogen), the pressure vessel was degassed (5 × nitrogen/vacuum). The vessel was heated to 53 °C, pressure purged with hydrogen gas (3 × hydrogen/vacuum), and placed under hydrogen gas (10 psig). The stirred slurry was aged overnight (~15 h) and then cooled to room temperature, and the pressure vessel was vented to atmospheric pressure. The reaction was determined to be complete (>99.9 area % conversion, 215 nm) by HPLC. Assay yield = 98.2% (2.46 g); ee = 91%.

K_{eq} Determination and r_{isom} for 1-E·TMG/1-Endo·TMG. A typical experiment was performed as follows: a Mettler-Toledo Multimax vessel equipped with overhead stirring, a port for reagent additions, and a sample line was charged with **1-E** (2.5 g, 5.7 mmol), MeOH (19 mL), and tetramethylguanidine (720 μL, 1.05 equiv). The solution was degassed with vacuum/nitrogen purges three times. Catalyst **3** (5.7 mL, 0.012 M) was added via the reagent addition port, and the solution was warmed to 50 °C. Samples were taken periodically until equilibrium had been reached (3 h). The equilibrium constant was measured by HPLC at 215 nm. $K_{eq(1)}$ was determined to be 0.29. The maximum rate of isomerization was determined by taking the derivative of the reaction samples over the course of the isomerization. The fastest rate of isomerization (r_{isom}) was determined to be 1.4 × 10^{-5} mol/L·s.

IR Kinetic Measurements. A typical experiment was performed as follows: in a glovebox, a Mettler-Toledo Multimax vessel equipped with overhead stirring, a port for reagent additions, and a sample line was charged with **1-E** (2.5 g, 5.7 mmol), MeOH (19 mL), tetramethylguanidine (720 μL, 1.05 equiv), and **3** (5.7 mL, 0.012 M). The vessel was sealed, removed from the box, and placed in a Multimax IR instrument. The agitation was initiated (1000 rpm), and the solution was warmed to 50 °C. The solution was subjected to H_2 (15 psig)/vacuum three times and then placed under H_2. The reaction was monitored by infrared spectroscopy and periodic sampling. Reaction concentrations were obtained by analysis of the samples by HPLC and correlated with the IR data. Reaction profiles were obtained by monitoring the absorbances at 1588 cm^{-1} (**1-E**) and 1625 cm^{-1} (**2**) and referencing each peak to two baseline points (1655 and 1509 cm^{-1}) which did not change with time. In general, spectra were acquired every 4 min at 4 cm^{-1} resolution with 128 scans.

Deuterium Labeling Experiments. A typical experiment was performed as follows: in a glovebox, a vial (8 mL) containing a stir bar was charged with **1-Endo** (100 mg, 0.23 mmol), CH_3OH (800 μL), tetramethylguanidine (29 μL, 0.23 mmol), and **3** (230 μL, 0.012 M). The vial was transferred to a resealable pressure vessel partially filled with sand. The vial was placed such that the solution was surrounded by sand. The pressure vessel was removed from the glovebox, placed in an oil bath preheated to 50 °C, and attached to a hydrogen/nitrogen/vacuum manifold. After the solution was subjected to three nitrogen (65 psi)/vacuum purges, the solution was exposed to D_2 (30 psi) for 2 h. The vessel was vented, and the resulting solution containing **2·TMG** was evaporated to dryness and redissolved in CD_3CN. ^{1}H NMR spectroscopic analyses were performed by first determining an appropriate delay time (typically 15 s) between pulses where integration values between signals remained constant. A total of 16 scans employing this delay were employed on the reaction sample. The aromatic C−H resonance ortho to the sulfone and fluoro groups was used as a reference signal (integration value = 1 proton). The β and γ protons were distinguished by TOCSY and gradient NOE experiments.

Acknowledgment. The reviewers are greatly acknowledged for their insightful comments on the content of this manuscript.

Supporting Information Available: Crystallographic information for **1-Endo**, representative kinetic data, complete hydrogenation screening data for **1-Br-E** and **1-E**, solubility data for **1-E**, and complete refs 14 and 26. This information is available free of charge via the Internet at http://pubs.acs.org.

JA0623358

(69) In the absence of hydrogen, methanolic solutions of **1-E·TMG** and **3** were found to liberate small quantities of the catalyst poisons dimethylamine and ammonia over 24 h (GC analysis). In order to maximize catalyst turnover, solutions of the catalyst **3** were added immediately prior to hydrogen addition.